AD-A078 894 TEXAS TECH UNIV LUBBOCK LASER LAB F/G 20/9
STUDIES OF TRANSIENT DISCHARGES.(U)
OCT 79 P F WILLIAMS , M A GUNDERSEN F49620-79-C-0118
UNCLASSIFIED AFOSR-TR-79-1304 NL

| OF |
AD A
078894

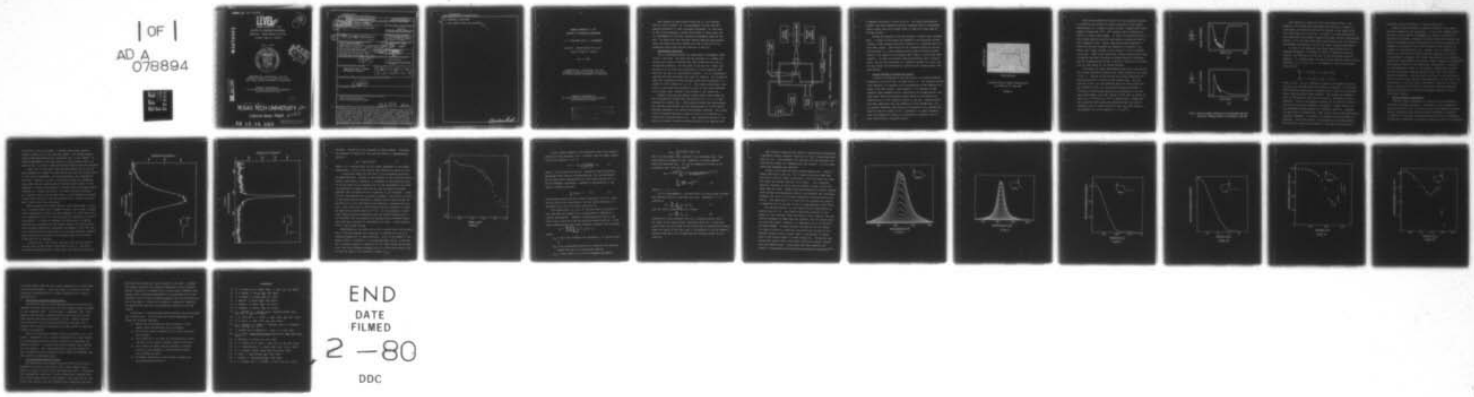

END
DATE
FILMED
2 -80
DDC

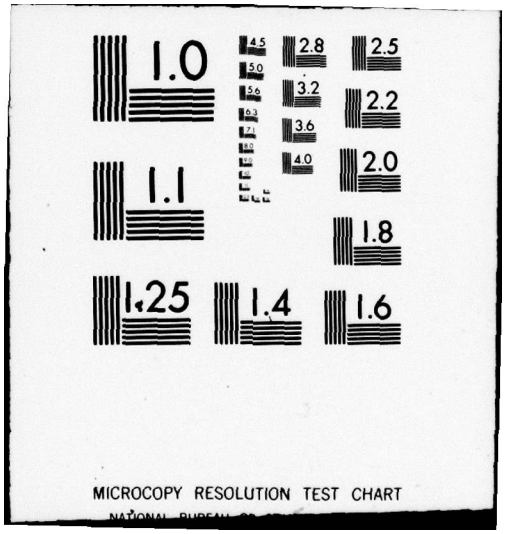
1.0
1.1
1.25
1.4
1.6
1.8
2.0
2.2
2.5
2.8
3.2
3.6
4.0
4.5
5.0
5.6
6.3
7.1
8.0
9.0
MICROCOPY RESOLUTION TEST CHART

LEVEL II

(17)

ANNUAL REPORT NO. 2 ON

STUDIES OF TRANSIENT DISCHARGES

GRANT NO. AFOSR F49620-79-C-0118

Project Task No. 2301/A7

Oct 1, 1979

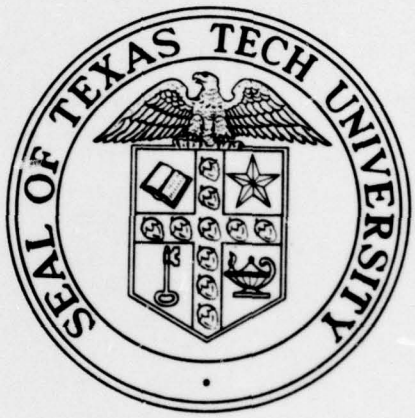

Research Sponsored by
Air Force Office of Scientific Research
United States Air Force

Laser Lab.

TEXAS TECH UNIVERSITY

Lubbock, Texas 79409

411518

UNCLASSIFIED

SECURITY CLASSIFICATION OF THIS PAGE (When Data Entered)

REPORT DOCUMENTATION PAGE

READ INSTRUCTIONS BEFORE COMPLETING FORM

1. REPORT NUMBER: AFOSR-TR-79-1304	2. GOVT ACCESSION NO. / 3. RECIPIENT'S CATALOG NUMBER
4. TITLE (and Subtitle): Studies of Transient Discharges.	5. TYPE OF REPORT & PERIOD COVERED: Interim, June 15, 1978 - June 14,
	6. PERFORMING ORG. REPORT NUMBER
7. AUTHOR(s): P.F. Williams and M.A. Gundersen	8. CONTRACT OR GRANT NUMBER(s): F49620-79-C-0118
9. PERFORMING ORGANIZATION NAME AND ADDRESS: Laser Laboratory, Department of Electrical Engineering, Texas Tech University, Lubbock, TX 79409	10. PROGRAM ELEMENT, PROJECT, TASK AREA & WORK UNIT NUMBERS: 2301/A7 61102F
11. CONTROLLING OFFICE NAME AND ADDRESS: (AFSC) Air Force Office of Scientific Research, Directorate of Physics (NP), Bolling Air Force Base, DC 20332	12. REPORT DATE: 1 Oct 79 / 13. NUMBER OF PAGES: 26
14. MONITORING AGENCY NAME & ADDRESS (if different from Controlling Office): A7	15. SECURITY CLASS. (of this report): Unclassified / 15a. DECLASSIFICATION/DOWNGRADING SCHEDULE

16. DISTRIBUTION STATEMENT (of this Report)

Approved for public release; distribution unlimited.

Annual rept. no. 2, 15 Jun 78-14 Jun 79

17. DISTRIBUTION STATEMENT (of the abstract entered in Block 20, if different from Report)

29

18. SUPPLEMENTARY NOTES

19. KEY WORDS (Continue on reverse side if necessary and identify by block number)

Laser Triggered Switch
Electrical Breakdown Model.

411518

20. ABSTRACT (Continue on reverse side if necessary and identify by block number)

Progress during the time period June 15,1978 through June 14,1979 in our program to study the basic physical processes responsible for laser-induced breakdown of spark gaps is reported. Major accomplishments during the period include (1) the measurement of temporally and spatially resolved electron densities during and after the arc phase, (2) the study of the initial buildup of charge and current in these gaps, and (3) improvements in the data acquisition equipment used in the work. Evidence of a shock front seen in the elec-

DD FORM 1473 EDITION OF 1 NOV 65 IS OBSOLETE

UNCLASSIFIED

20. ABSTRACT (continued)

tron density data was obtained.

ANNUAL REPORT NO. 2 ON

STUDIES OF TRANSIENT DISCHARGES

P. F. WILLIAMS and M. A. GUNDERSEN

Grant No. AFOSR F49620-79-C-0118

Project Task No. 2301/A7

Oct 1, 1979

Research Sponsored by
Air Force Office of Scientific Research
United States Air Force

Work during the grant period from June 15, 1978 through June 14, 1979 included: (1) the measurement of time resolved electron densities in laser triggered discharges, (2) the study of the initial buildup of charge and current in these gaps, and (3) improvements of the data acquisition equipment used for this work. An effort was also directed towards studying spectroscopically the events occurring between the time of arrival of the triggering laser pulse and the formation of the arc.

1. Experimental Apparatus

For all discharge studies the experimental arrangement shown in Fig. 1 was used. The spark gap was enclosed in a vacuum container which could be evacuated and then backfilled with gas to the desired pressure. One electrode of the gap had a small hole drilled in it to allow the introduction of the triggering laser beam into the gap in a longitudinal geometry. For all experiments reported here the electrodes were made of aluminum. The triggering laser was a Molectron UV-400 nitrogen laser which delivered 5 mJ pulses of 3371 Å radiation in 10 ns. The roughly rectangular (spatially) output beam was focused to a point on the lower electrode with a quartz lens, through a CaF_2 window in the vacuum cell.

Emission from the gap passed through another CaF_2 window and was collected and focused onto the entrance slit of a 0.5 m spectrograph by a quartz lens. After passing through the spectrograph, the radiation was focused onto the photocathode of an SIT vidicon detector connected to an optical multichannel analyzer. This setup allows a spectrum covering a range of 200 Å to be acquired in a single shot with good sensitivity. The intensifier section of the SIT may be gated, allowing time-resolved data to be acquired with

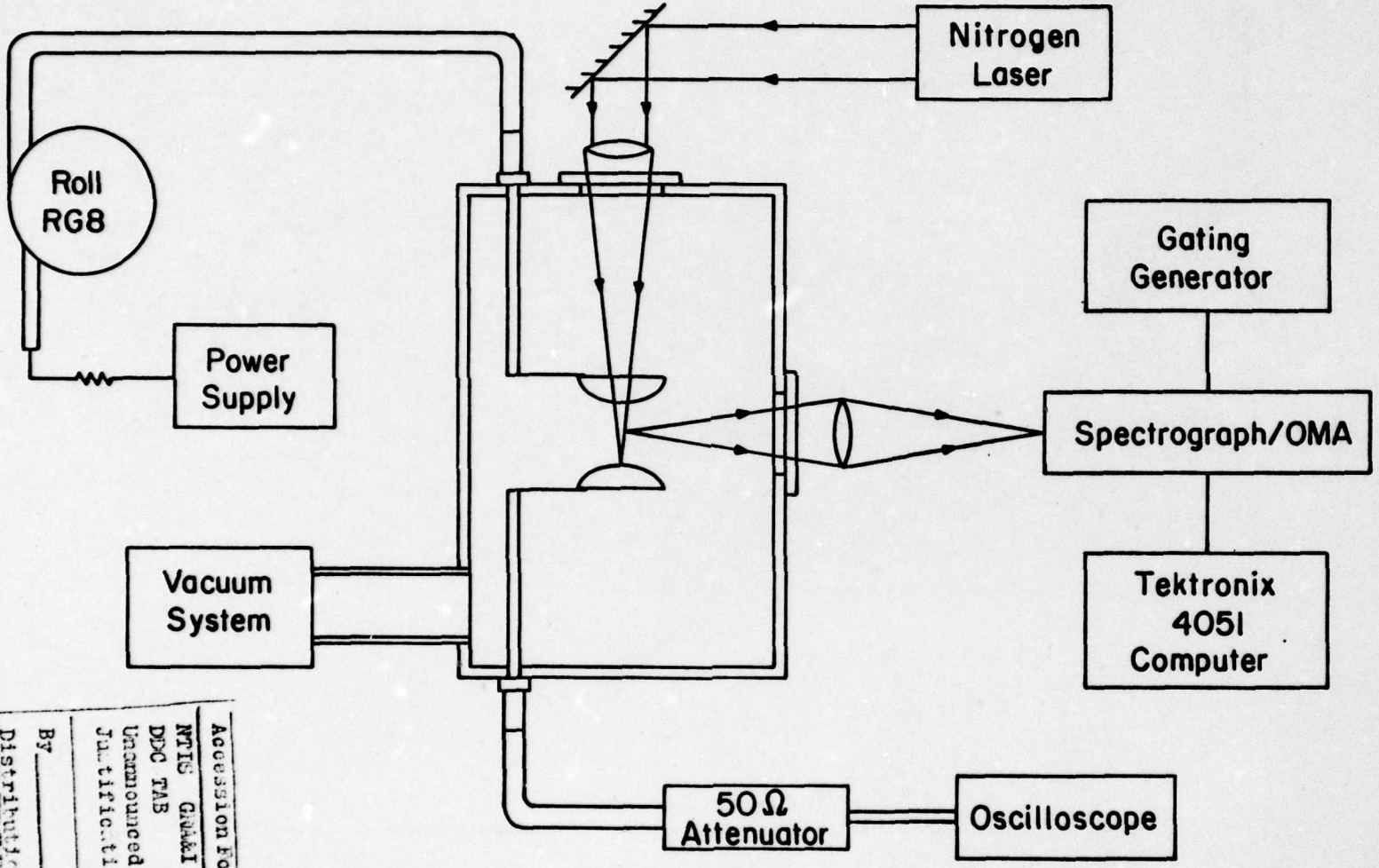

Fig. 1. Schematic drawing of experimental setup.

a temporal resolution of down to 50 ns. For these time-resolved studies, the gate generator could be triggered after an adjustable delay, either from the nitrogen laser or from the rising edge of the gap current.

Voltage was applied to the gap through a charged cable arrangement. A length of RG-8 cable was charged to the operating voltage through a large charging resistor connected to a regulated high voltage power supply. Application of the triggering pulse to the gap then resulted in a nicely shaped current pulse of duration proportional to the length of the charged cable (about 1 μs for most experiments). In order to minimize waveform distortion due to reflections, the gap was terminated in a carefully matched 50 Ω load, and the gap current was determined by measuring the voltage across this load resistor.

2. Initial Buildup of Charge and Current

A typical oscillogram of the gap current in a laser-triggered discharge in H_2 at 350 Torr is shown in Fig. 2. The observed current rises smoothly to a maximum value corresponding to the complete collapse of the gap voltage. This behavior is in contrast to that observed under somewhat similar conditions with conventionally triggered gaps, where well-defined current steps or even maxima are observed prior to the complete closure of the gap. These features have been associated with the formation of the cathode fall, the arc channel formation, and finally the bridging of the cathode fall region by the arc channel [1-5]. Apparently, in laser triggered gaps, the sequence of events is significantly different than in more conventionally triggered devices.

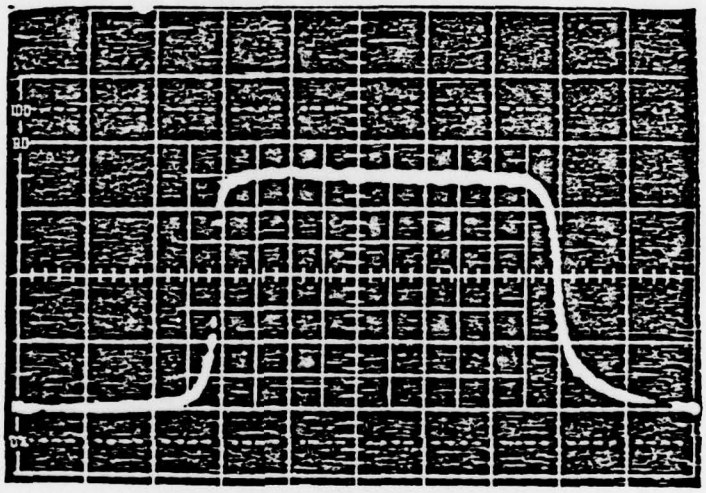

CURRENT PULSE IN LASER–TRIGGERED GAP.
H_2 at 350 Torr, 5 kV, 50Ω load.

FIGURE 2.

The primary difference between the two triggering methods is related to the amount of charge liberated by the trigger. Conventional U.V. trigger sources provide a comparatively small number of electrons (10^2 - 10^3) whereas laser triggering results in a much larger number. In order to characterize better the initial pulse of positive and negative charge provided by the triggering laser, initial experiments were conducted in which the gap was evacuated as completely as possible (<0.1 mTorr) and a small voltage in the range of 0 to 20 V applied to the gap. Under those conditions, charge multiplication from ionization and other secondary processes should be minimized, and the integrated gap current should be a measure of the quantity of free charge in the plasma fireball.

The results of these experiments proved quite interesting. Two current waveforms observed under these conditions are shown in Fig. 3. Figures 3a and 3b show the current observed with plus and minus 23 V across the gap respectively. For the polarity in Fig. 3a, the positive charge is drawn across the gap, whereas in Fig. 3b, the negative charge traverses it. In spite of the striking qualitative differences in the current pulse shapes, the total charge in each case is nearly the same (2.8×10^{-8} and 2.4×10^{-8} C, respectively), supporting the contention that charge multiplication does not play an important role in these results and that the total charge in the fireball is in the range of $2 - 3 \times 10^{-8}$ C.

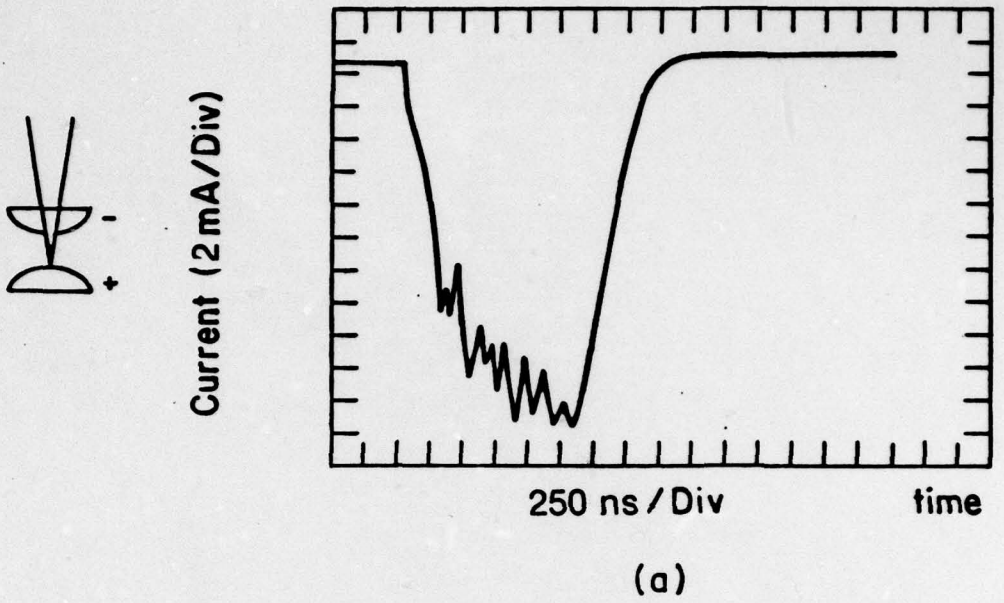

(a)

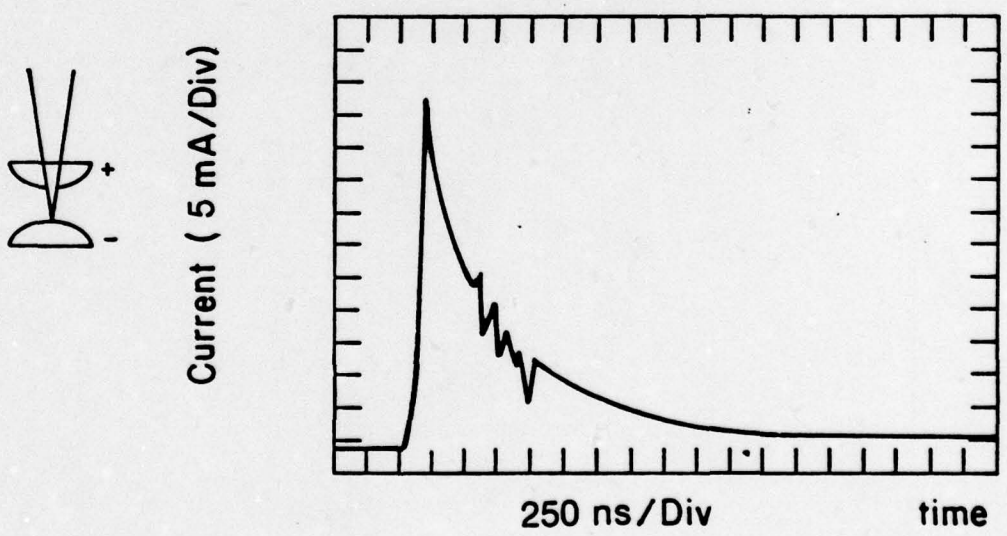

(b)

Fig. 3. Current pulses observed in an evacuated gap with ±23 volts. Voltage polarity is indicated on the left.

This quantity of charge can have significant effects. For example if the charge were unshielded and confined to a sphere of 1 mm radius, the electric field at the surface of the sphere would be of the order of 2×10^6 V/cm. Of course, in these experiments, such fields are not produced, because the plasma remains approximately neutral, but it is clear that space charge effects play an important, and probably even dominant role in our laser triggered experiments.

In light of the important role space charge effects play in breakdown phenomena, a theoretical effort to understand them was recently initiated and is to be part of the continuing program of research. In a simple model, the positive and negative charge carrier densities, $\rho_+(r,t)$ and $\rho_-(r,t)$, are expected to obey the following relations [6]

$$\frac{\partial \rho}{\partial t} = -\mu_+ \vec{\nabla}\cdot(\rho_+ \vec{E}) - \alpha \mu_- \rho_- |\vec{E}| + D_+ \nabla^2 \rho_+$$
$$\frac{\partial \rho}{\partial t} = -\mu_- \vec{\nabla}\cdot(\rho_- \vec{E}) + \alpha \mu_- \rho_- |\vec{E}| + D_- \nabla^2 \rho_- \qquad (1)$$

where ρ_+ and ρ_- are the densities of positive and negative charge, $\mu_\pm$ and $D_\pm$ are the mobilities and diffusion constants, α is the Townsend ionization coefficient (a function of $\vec{E}$), and $\vec{E}$ is the electric field, including space charge effects. The charges are assumed to drift in the electric field and to diffuse in response to density gradients. Positive and negative charges may be created by ionization of gas molecules (Townsend α processes). Charge creation at the electrode surfaces appears as a boundary condition. Although not specifically included here, other effects such as photoionization, electron attachment, or negative ion production could be added as necessary. Since the electric field depends on the charge density, both the drift term and the Townsend α term make these equations

non-linear, and very difficult to solve analytically.

Efforts toward developing a computer program to solve these equations numerically are continuing. In this work, symmetry about the axis of the discharge is assumed, but radial variations are specifically included. Kohrmann and others [6-9] have reported the results of somewhat similar calculations in which the discharge was assumed to be uniform in the radial direction, thus reducing the problem to a one-dimensional one. However, such an assumption is clearly not justified for laser-triggered discharges, and radial non-uniformity is essential for proper description of the phenomena. Yoshida and Tagashira[10] and later Davies, Evans, Townsend, and Woodison[11] have reported results of two dimensional calculations. Because of the two-dimensional nature of the problem, considerable care must be taken to minimize computer execution time, and, particularly, memory requirements. The problem is most acute in the calculation of the electric field from the charge densities. At the end of the grant period, we had not found a satisfactory solution to the problem of calculating the electric field which required reasonable computer resources while providing acceptable accuracy. Work is continuing, however.

3. Electron Density Measurements

Electron density information is important for understanding electrical breakdown processes. Accordingly, Stark broadening of the H_α and H_β lines was utilized to obtain time dependent electron density information from laser-triggered discharges in hydrogen. In addition to measuring the electron density during the discharge, we were also interested in determining densities after the termination

of the arc. For this purpose, a voltage source which could be rapidly turned off at a set time was needed. The charged coaxial cable system described earlier functioned well in this regard. By careful adjustment of the load resistor a clean current pulse, as shown in Fig. 2, with no reflection-induced after-pulses was obtained.

Using a 50 ns wide gate, time resolved spectra of the H_β line were obtained at a number of times during and after the current pulse. In the initial experiments, the gating generator was triggered by the laser. Because of jitter in the delay between the triggering laser pulse and the leading edge of the gap current pulse, it was necessary to record a spectrum and a current pulse oscillogram simultaneously on a single shot basis. In order to obtain a spectrum at a specific time in the current pulse, it was necessary to monitor several such shots until one was obtained with a current pulse properly lined up with the gate pulse.

Besides making data taking tedious, this problem made it difficult to signal-average over a number of shots, and it made it essentially impossible to obtain the data necessary for using Abel inversion techniques [12-14] to unfold the spatial variation of the electron density. In order to overcome this difficulty, the gating generator was triggered from the leading edge of the current pulse. This procedure essentially eliminated the temporal jitter but, due to an internal delay of about 100 ns in the gate generator, measurements during the early parts of the leading edge of the current pulse could not be obtained.

Figures 4 and 5 show typical spectra of the H_β line seen at various times in the current pulse shown in Fig. 2. The first spectrum was obtained from a single shot, the second is the sum of

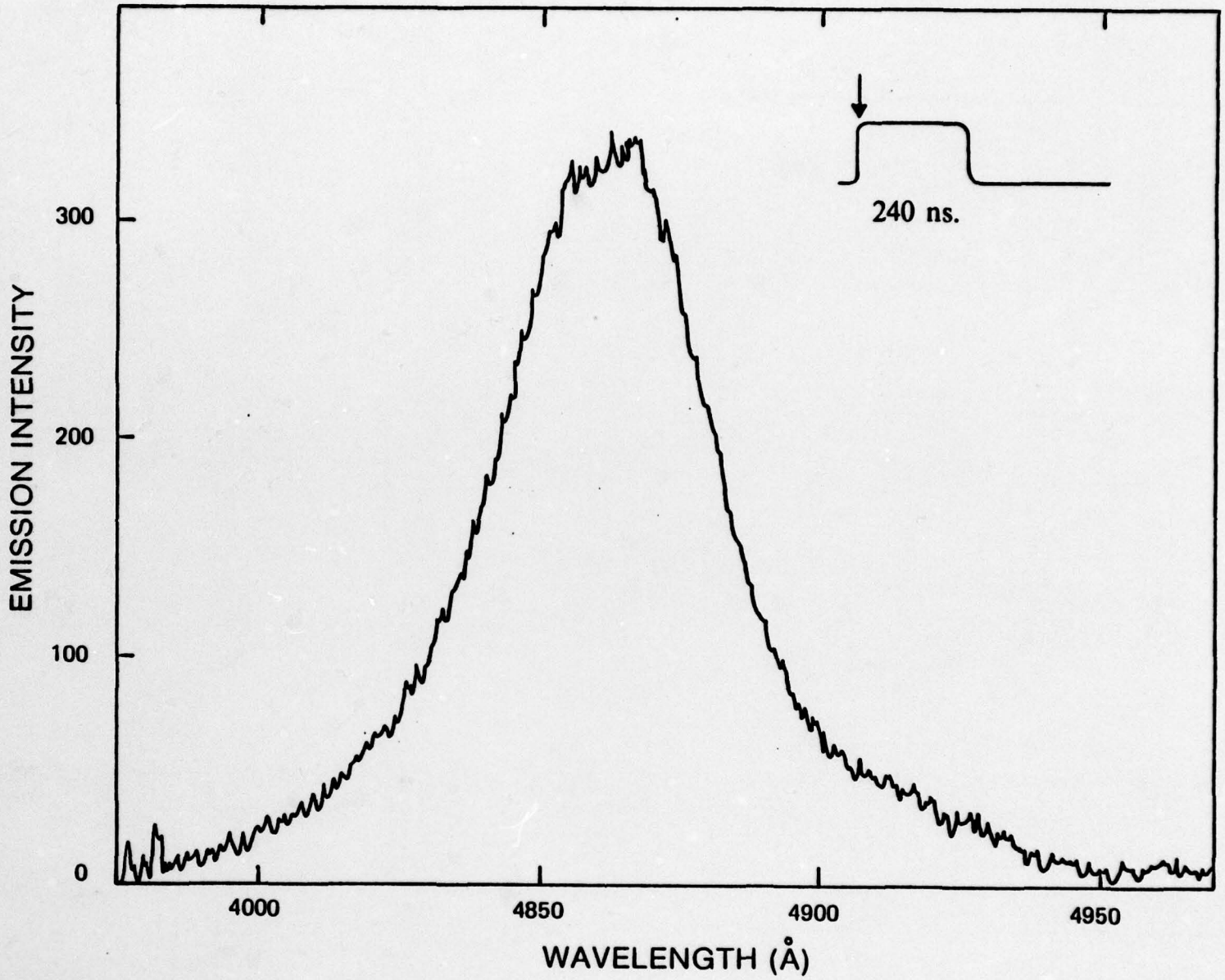
EMISSION INTENSITY
300
200
100
0
4000
4850
4900
4950
WAVELENGTH (Å)
240 ns.

FIGURE 4.

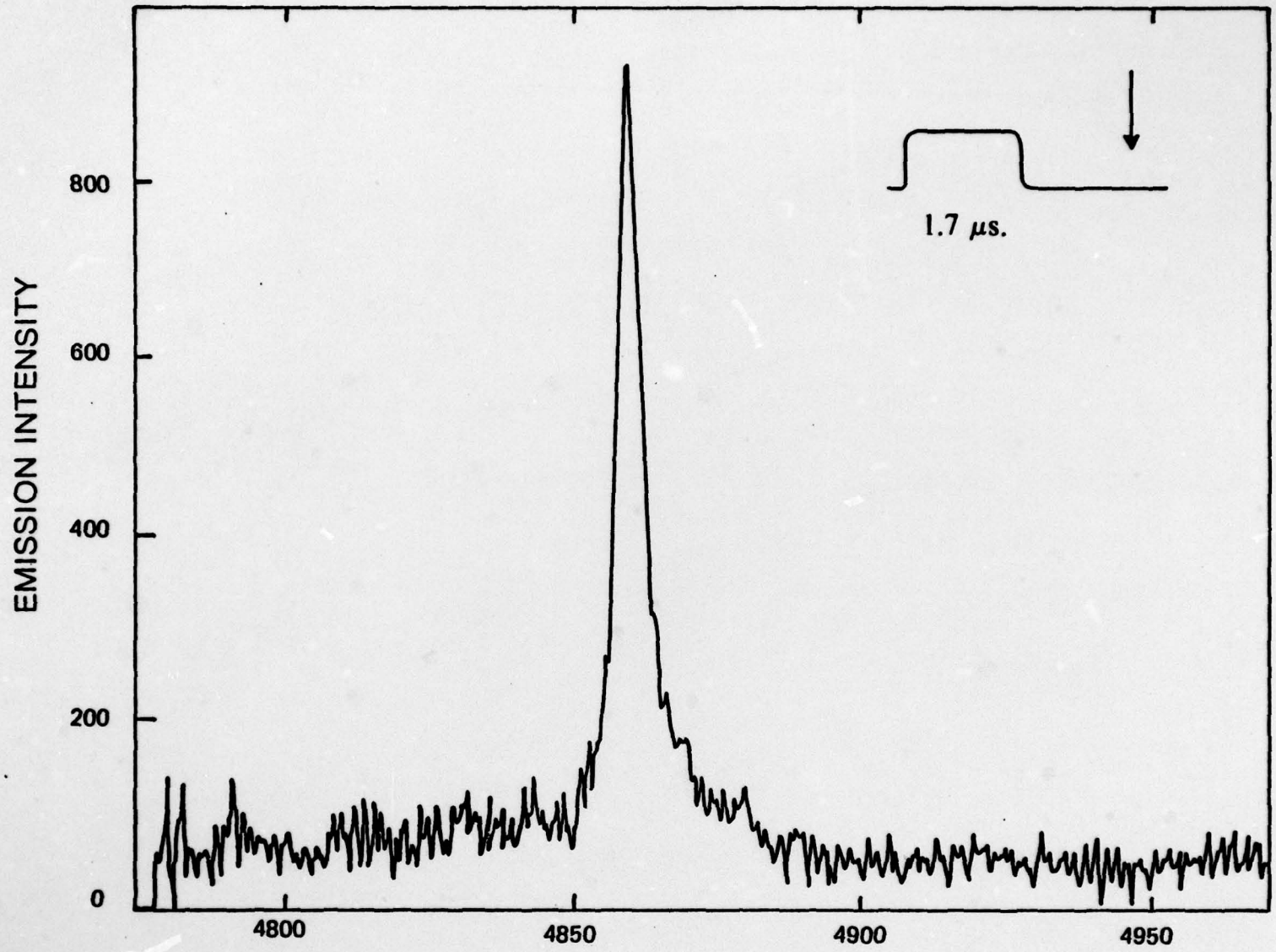
EMISSION INTENSITY
800
600
400
200
0
4800
4850
4900
4950
WAVELENGTH (Å)
1.7 μs.

FIGURE 5.

20 shots. Variation of the linewidth is quite evident. Following the analysis of Griem [12], the electron density is approximately given by

$$N_e = C(N_e,T)\nabla\lambda_s^{3/2} \qquad (2)$$

where C is a constant which is only weakly dependent on the plasma temperature. A plot of the density thus obtained is shown in Fig.6.

It should be noted that the data in Fig.6 represent spatially averaged densities. Because of the geometry of the collection optics system, high spatial resolution is available in the direction parallel to the plane of the entrance slit of the spectrometer, but there is essentially no depth resolution so that the spectra obtained represent data averaged over this dimension of the discharge. Assuming that the discharge has cylindrical symmetry, the radial variation of the spectra may be unfolded by stepping the arc image across the entrance slit of the spectrograph and obtaining a spectrum for each step. With these data, an Abel inversion may be performed to obtain the spatially resolved spectra [12-15]. For this purpose, an efficient computer program compatible with the limited capabilities of our Tektronix 4051 minicomputer was developed for performing numerically the Abel inversion of experimental raw data. A brief description of the program follows.

Experimentally, the image of the arc is moved across the entrance slit of the spectrograph and a spectrum is obtained for each of a regularly-spaced net of image positions. If N_λ is the number of frequency points, or channels, in a single spectrum, and N_x is the number of spectra acquired in sweeping the arc image across the entrance slit, then this procedure produces an $N_x \times N_\lambda$ data matrix which constitutes the input to the inversion program, $I_{n_x n_\lambda}$.

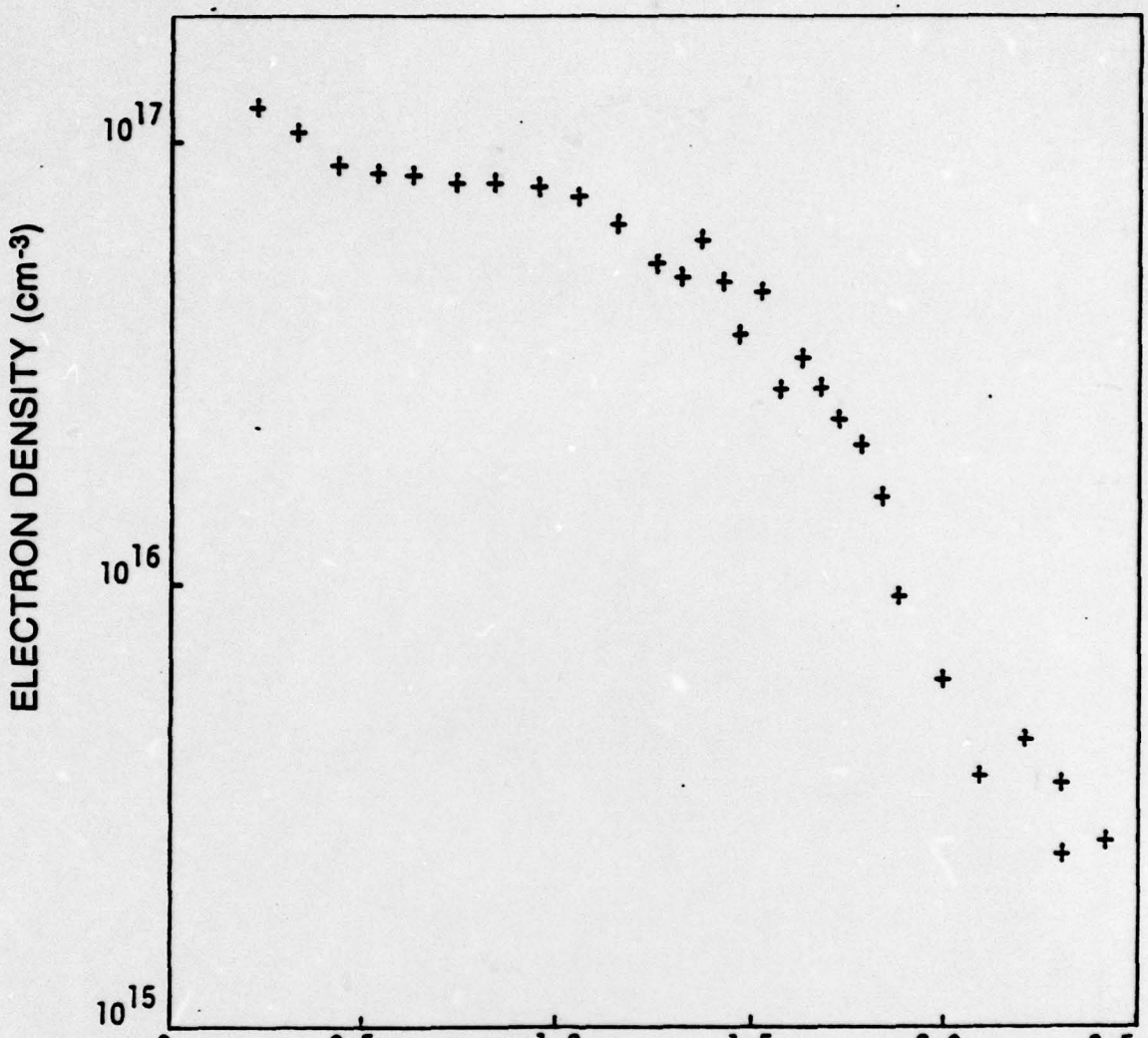

FIGURE 6.

If for a given frequency, the functional form of the lateral variation of the intensity, I(x), is known, then the radial variation of the intensity, $\varepsilon(r)$ is

$$\varepsilon(r) = -\frac{1}{\pi}\int_{r}^{r_o}\frac{I'(x)}{\sqrt{x^2 - r^2}}\,dx \qquad (3)$$

where r_o is the radius of the arc. Because of the difficulties associated with numerical differentiations, for each frequency, the N_x data points representing I(x) were least-squares fit to a sum of Chebyshev polynomials, yielding an approximation to the lateral intensity function,

$$\sum_j a_j T_j(x) \simeq I(x) \qquad (4)$$

The necessary derivative and integral operations in eq (3) could then be carried out analytically, and the radial emission, $\varepsilon(r)$ evaluated for a set of N_r radial positions, r_ℓ.

The coefficients, a_j in eq (4) are most easily evaluated if the input data are spaced with a cosinusoidal as opposed to a regular distribution. Quadratic interpolation was used to construct such a data set from the regularly-spaced input set. With these considerations, the radial emission intensity matrix becomes

$$\varepsilon_{mi} = \sum_{j=1}^{N_x}\sum_{k=1}^{N_x}\sum_{\substack{\ell=0 \\ \ell \text{ even}}}^{L} B_{m,\ell}\, T_{\ell,k}\, S_{kj}\, I_{ji}$$

where:

I_{ji} is the input intensity for frequency λ_i at lateral point x_j.

S_{kj} is an interpolation matrix for converting the regularly spaced data set to a cosinusoidal spacing.

$T_{\ell h} = T_\ell(x_k)$ where T_ℓ is the ℓth Chebyshev polynomial.

$$B_{m,\ell} = \int_{r_m}^{r_o} (x^2 - r_m^2)^{-\frac{1}{2}} T_\ell'(x)\, dx$$

and L is the highest order included in the polynomial sum. Only even terms are included in the ℓ summation to ensure symmetry about the discharge axis. $B_{i\ell}$ can be computed by writing T_ℓ as an explicit sum, with the result[16]

$$B_{m\ell} = \ell\sqrt{1-r_i^2} \sum_{j=0}^{\ell/2-1} (-1)^j \frac{(\ell-j-1)!\,(\ell/2-j-1)!^2}{j!\,(\ell-2j-1)!^2}\, 2^{\ell-2j-1} \cdot$$

$$\sum_{k=0}^{k_o} \frac{(2k)!}{k!^2} (4r_m^2)^{k_o-k} \qquad (6)$$

where $k = \ell/2 - j - 1$.

For all wavelengths, λ_i, the matrices $\underline{\underline{S}}$, $\underline{\underline{T}}$, and $\underline{\underline{B}}$ remain constant and therefore need be calculated only once. Therefore if C is defined by

$$C_{mj} = \sum_{k=1}^{N_x} \sum_{\substack{\ell=0 \\ \ell \text{ even}}}^{L} B_{m\ell}\, T_{\ell k}\, S_{kj} \qquad (7)$$

then the radial emission matrix is simply

$$\epsilon_{ik} = \sum_{j=1}^{N_x} C_{ij}\, I_{jk} \qquad (8)$$

Evaluation of this expression for all N_λ spectral points (500 in our case) and N_r radial points (typically about 20) is then relatively fast, but the volume of data which must be manipulated severely taxes the limits of the 4051, and it is necessary to use the magnetic cassette tape drive for intermediate data storage during the calculation.

The inversion algorithm was tested by analytically constructing a synthetic lateral intensity function I(x) from a chosen functional form for $\varepsilon(r)$. This synthetic I(x) was fed into the inversion routine and the output $\varepsilon(r)$ compared with the original. For all cases tested the agreement was excellent.

Figure 7 and 8 show the Abel inverted spectra for a range of radial positions in the arc. Fig. 7 results from data taken near the start of the arc phase (t=150 nsec.), and Fig. 8 from data taken just after the current shut-off (t=1.2 usec.). The integrated spectral intensity of the H_β line is plotted in Figs 9 and 10 for these same two times. These curves were obtained by drawing straight lines through the experimental points, and therefore they accurately represent the noise in the signal acquisition and manipulation processes. From these data it is clear that the luminous arc channel is expanding with an average velocity of approximately 5×10^4 cm/sec.

The electron density, N_e, was found from the experimental H_β spectra using eq (2). The electron densities obtained in this manner for two different times are shown in Figs 11 and 12. The temperature assumed for these data was 20,000°K, but the results would not have been greatly affected if a temperature of up to 40,000°K had been assumed. In these results, the edge of the arc channel is clearly visible at a position consistent with the edge of the luminous column as seen in Figs 9 and 10. Additionally a second peak in the electron density is seen further out. We believe this second peak results from a shock wave travelling radially outward from the channel center. Shock waves have been observed very clearly in experiments using Schlieren photographic techniques,[17-19]

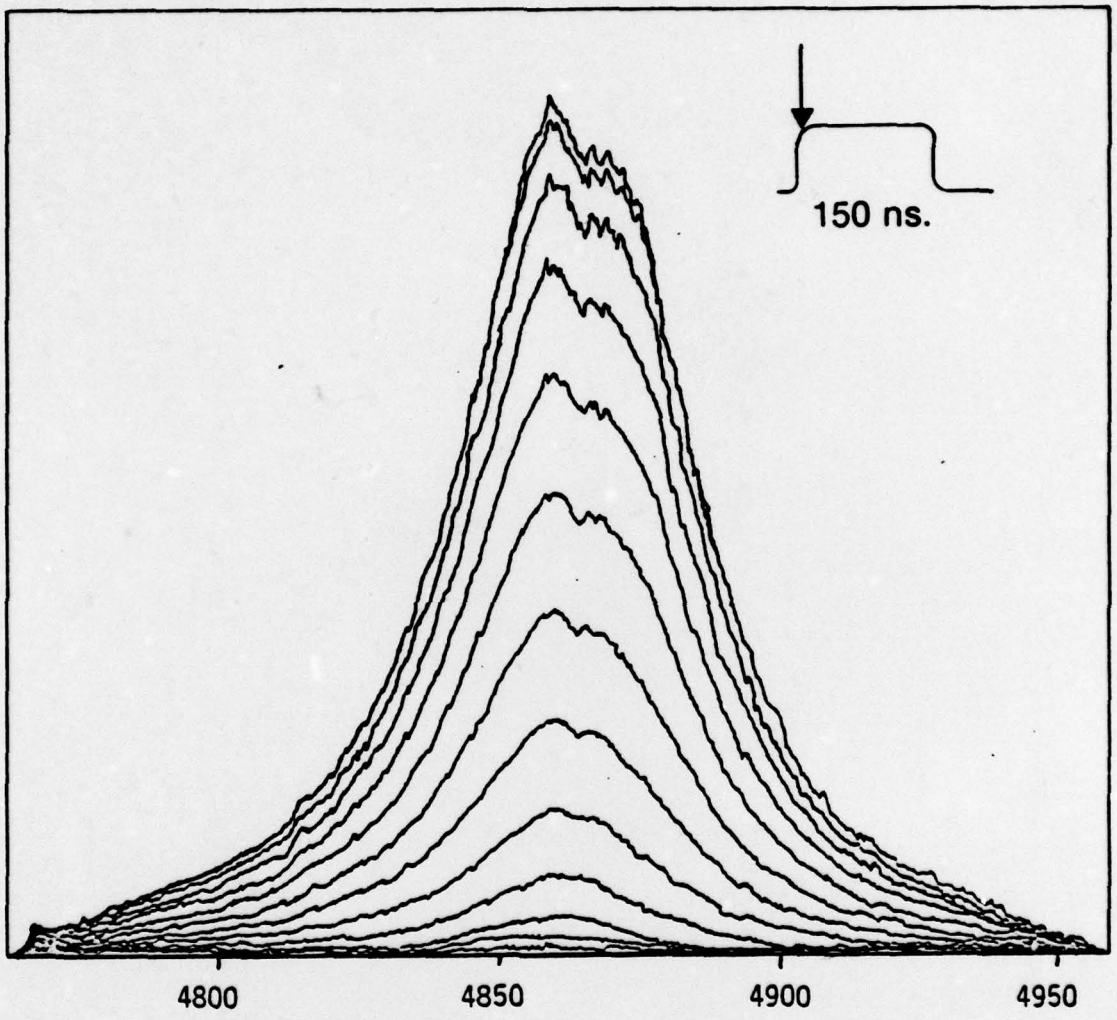

FIGURE 7.

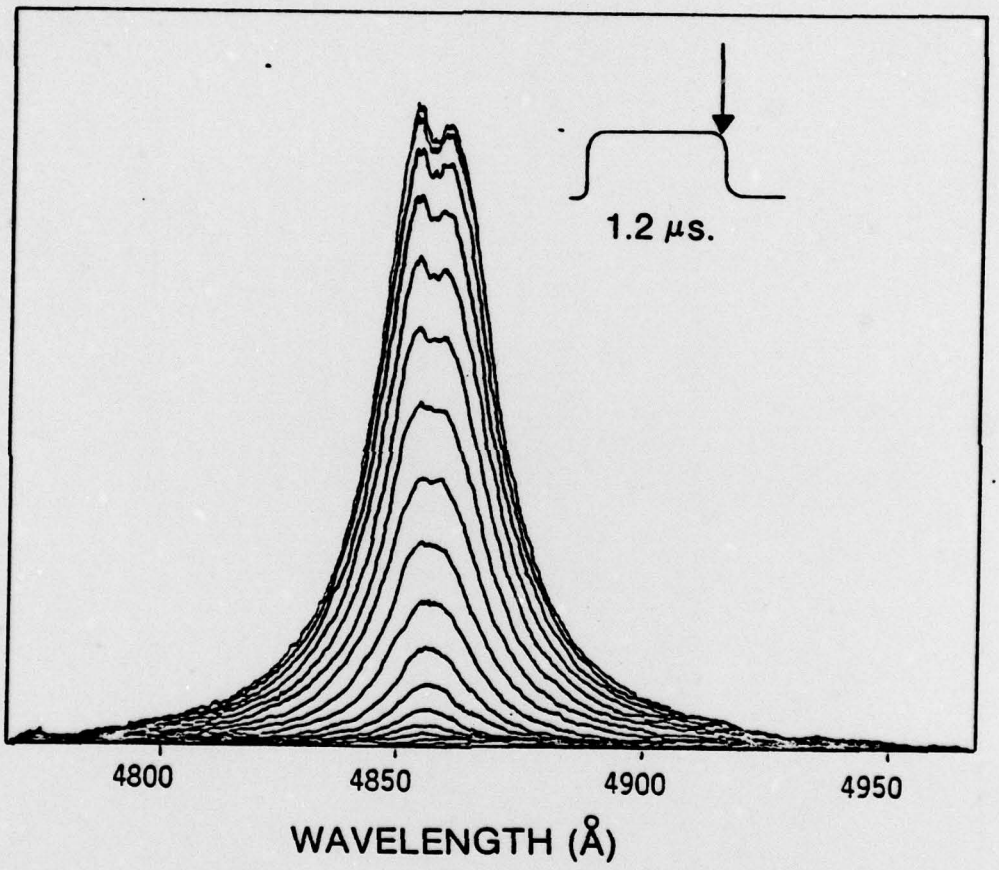

FIGURE 8.

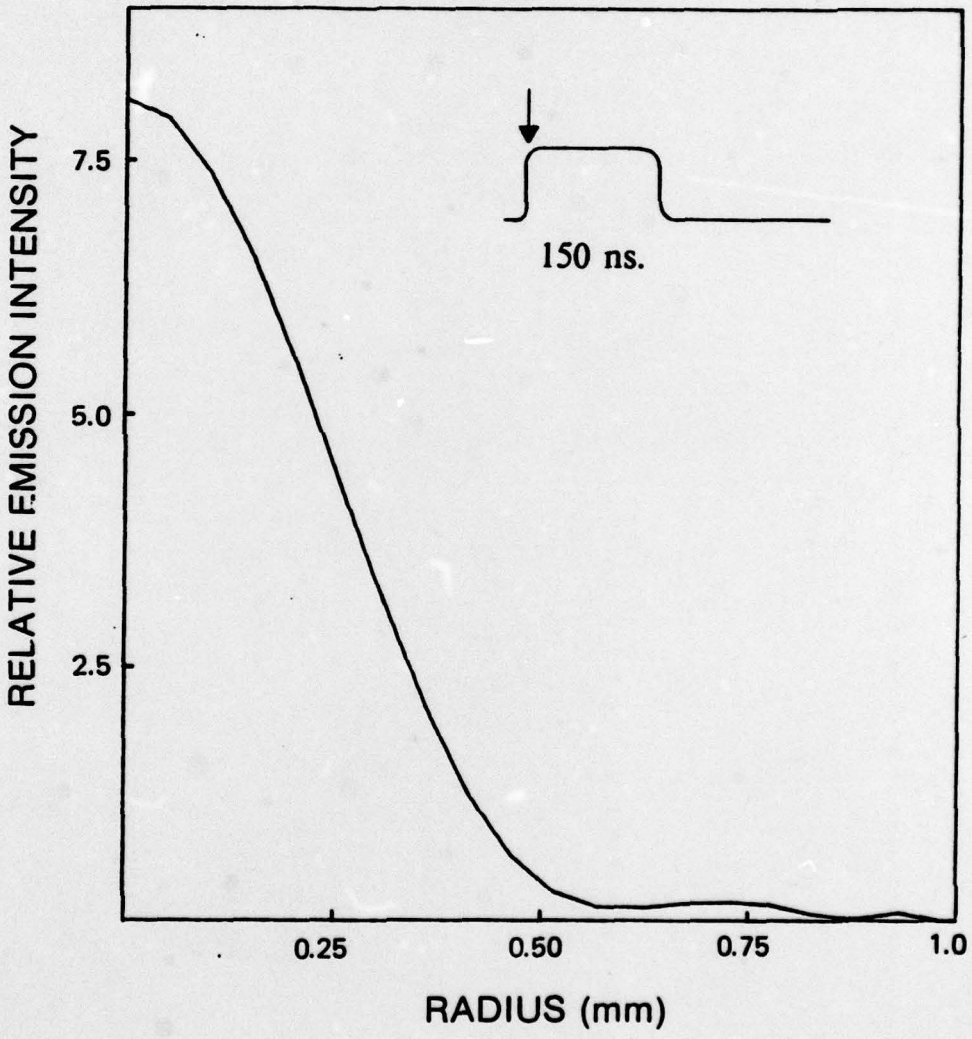
RELATIVE EMISSION INTENSITY
7.5
5.0
2.5
150 ns.
0.25
0.50
0.75
1.0
RADIUS (mm)

FIGURE 9.

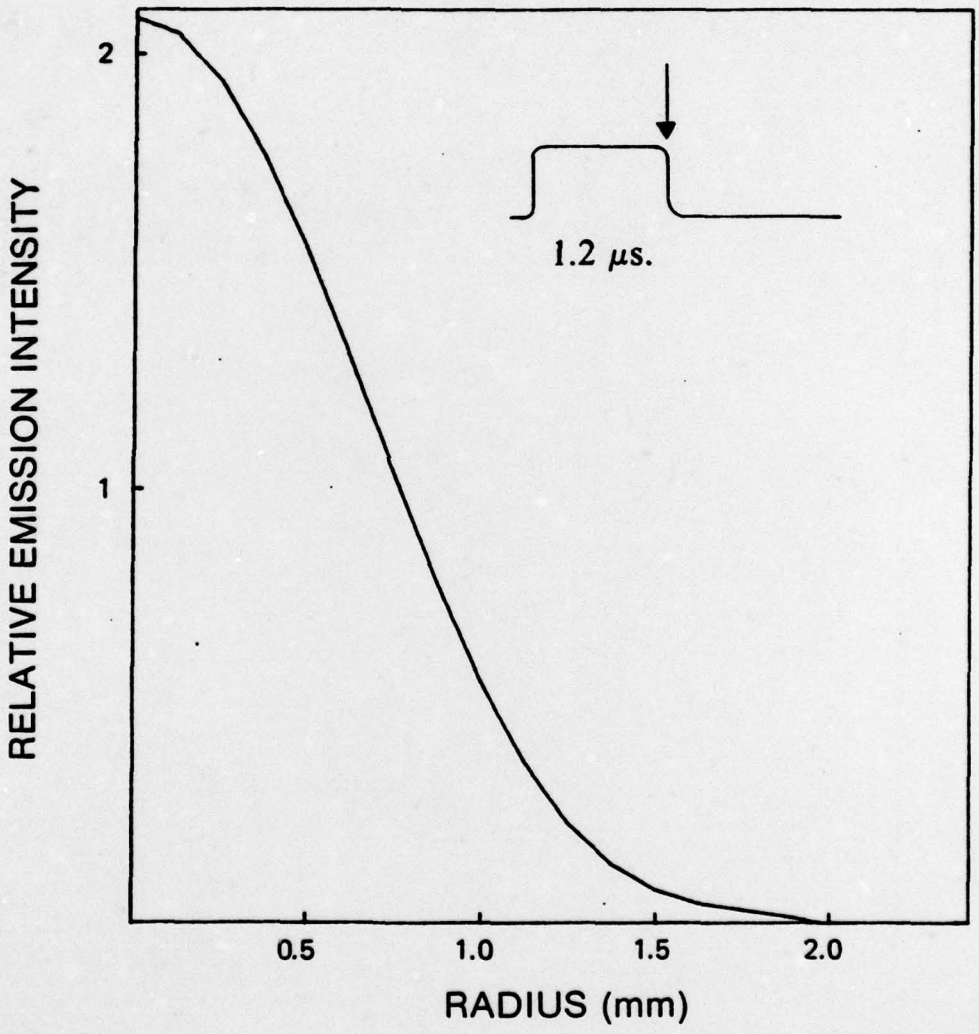

FIGURE 10

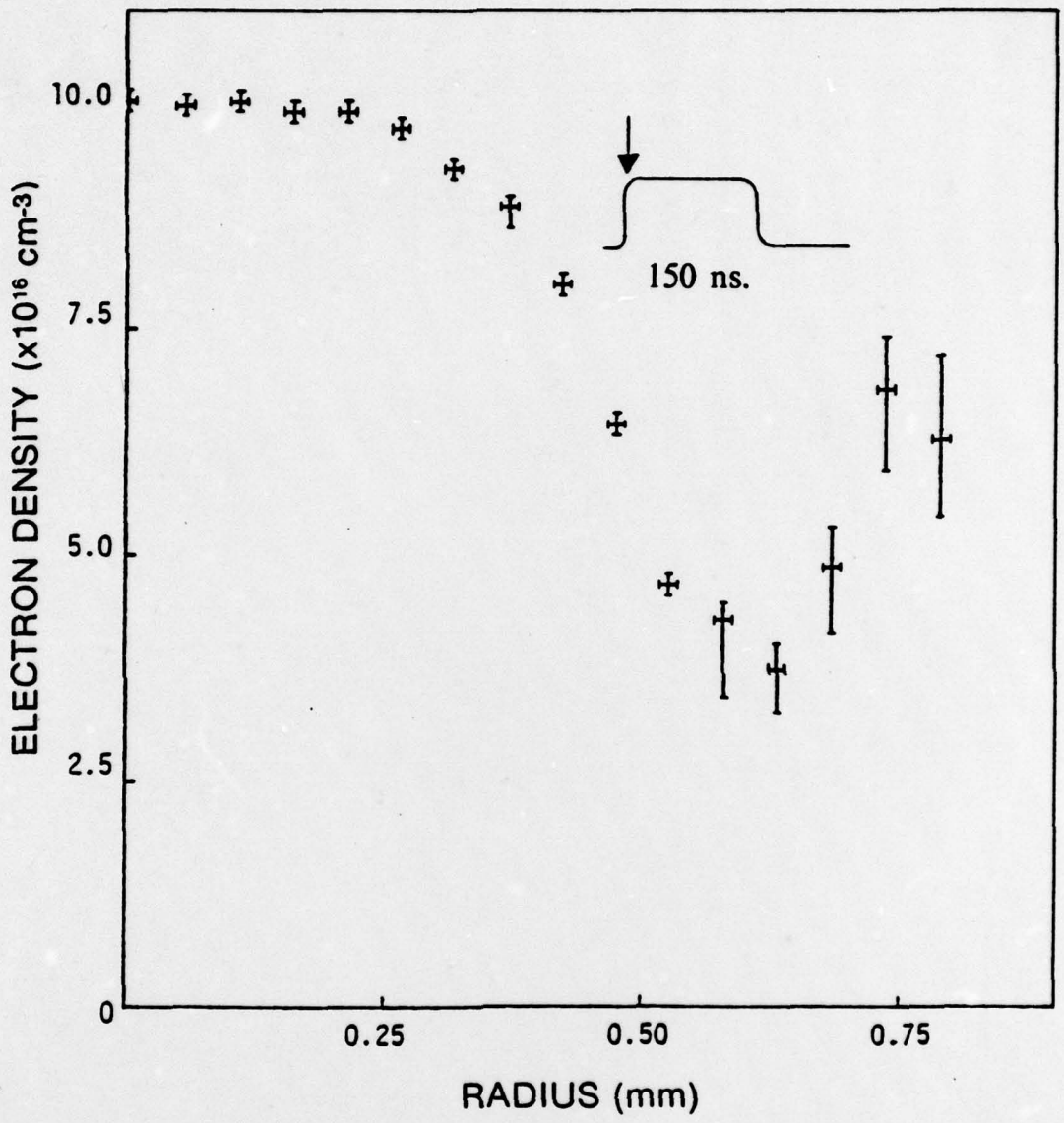
10.0
7.5
5.0
2.5
0
ELECTRON DENSITY (x10¹⁶ cm⁻³)
150 ns.
0.25
0.50
0.75
RADIUS (mm)

FIGURE 11.

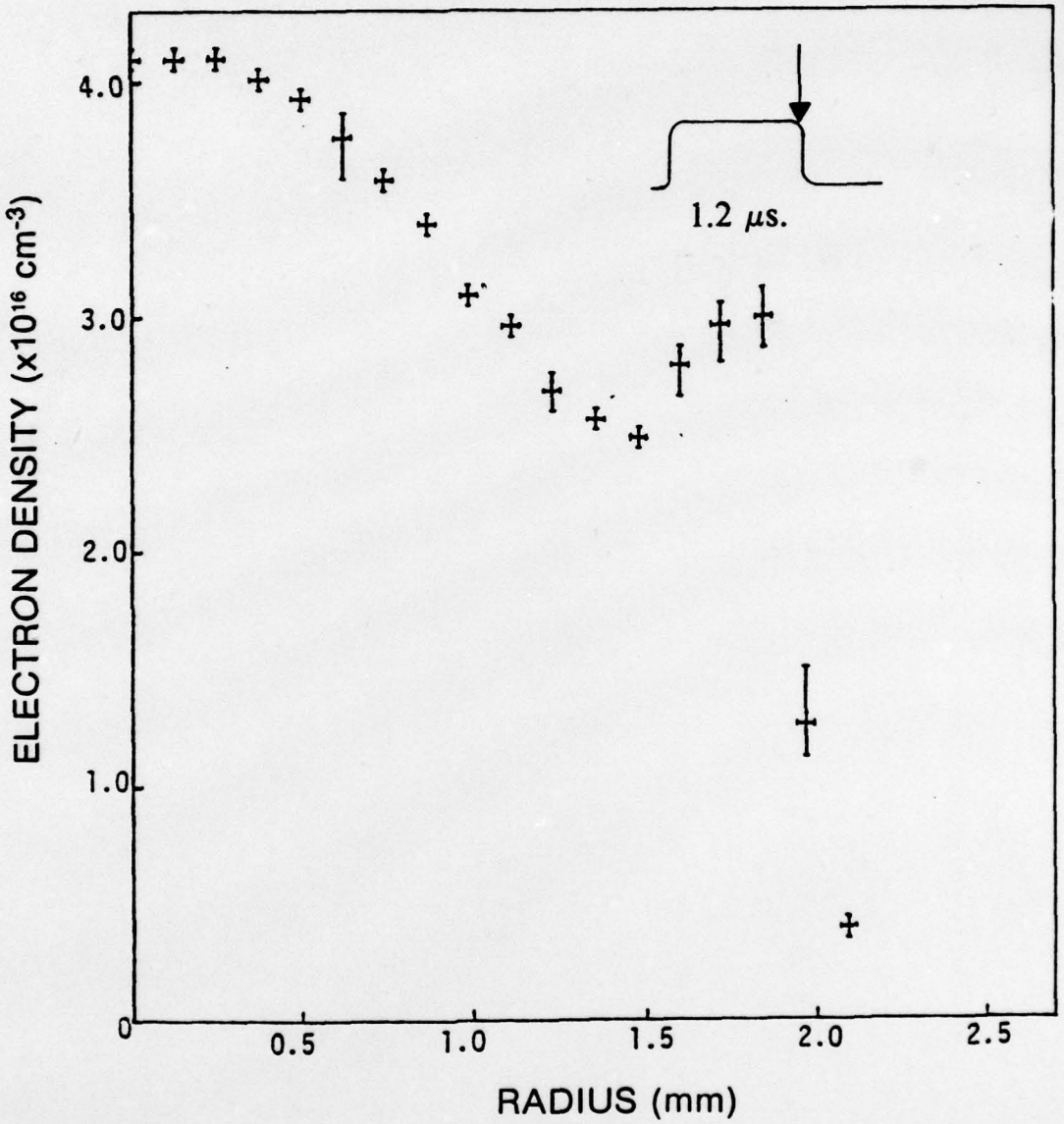
ELECTRON DENSITY (x10¹⁶ cm⁻³)
4.0
3.0
2.0
1.0
0
0.5
1.0
1.5
2.0
2.5
1.2 μs.
RADIUS (mm)

FIGURE 12.

but these results mark the first clear observation of a shock wave in the electron density. More work needs to be done to put the shock wave interpretation on a firmer foundation and to better characterize it.

4. Early-Time Fluorescence Measurements

An effort was made to study spectroscopically the early-time sequence of events starting with the small plasma fireball produced by the triggering laser. Unfortunately, in hydrogen, very little emission from the gap is observed during these times [1] so that these efforts have been unsuccessful to date. Several emission lines associated with the electrode material were seen, but no emission which could be identified with either atomic or molecular hydrogen was observed.

Much of the molecular hydrogen emission spectrum is in a continuum. Measurement of the emission spectrum with a lower dispersion spectrograph should be useful, therefore, in enhancing the detected intensity. A coarser grating has recently been acquired for this purpose. Also, other gases such as N_2 are reported to have a brighter emission during the early phases of breakdown, and they should be investigated also.

5. A Microprocessor-Based Interface

The PAR optical multi-channel analyzer which we are using is designed to be used in conjunction with a small computer which serves to control it and to store and manipulate data. A Tektronix 4051 minicomputer along with a locally constructed interface unit are currently being used for this purpose. Since the 4051 is relatively slow, during a run the interface must accumulate and store

data from the analyzer for later transfer to the 4051. Although the present interface unit performs adequately in this function, greater flexibility is needed both to allow simple arithmetic operations such a background subtraction to be performed within the interface, and to allow for memory expansion and for more efficient use of the memory. Better use of memory is especially important for applications requiring two-dimensional scanning of the OMA vidicon.

Accordingly, a microprocessor-based interface unit was designed and is being built. The unit uses the Z-80 microprocessor and offers the following features:

(1) Memory may be expanded by simply plugging in more memory cards and modifying the Z-80 program.

(2) Data may be stored in words of one to three eight-bit-byte lengths.

(3) Data transfers to the 4051 are facilitated by putting the data in the correct internal format of the 4051.

(4) The contents of memory may be displayed in graphic form on an oscilloscope or chart recorder without going through the 4051.

(5) Arithmetic operations on data stored in memory may be accomplished internally.

REFERENCES

(1) M. C. Cavenor and J. Meyer, Aust. J. Phys. 22, 155 (1969).

(2) K. H. Wagner, Z. Physik 189, 465 (1966).

(3) K. H. Wagner, Z. Physik 204, 177 (1967).

(4) J. Koppitz, Z. Naturf 229, 1089 (1967).

(5) J. Koppitz, Z. Naturf. 269, 700 (1971).

(6) W. Korhmann, Z. Naturf. 199, 926 (1964).

(7) A. J. Davies, C. J. Evans, and F. Llewellyn-Jones, Proc. Roy. Soc. A, 281, 164 (1964).

(8) L. E. Kline and L. J. Dines, J. Appl. Phys. 46, 1567 (1975).

(9) L. E. Kline, J. Appl. Phys. 46, 1994 (1975).

(10) A. J. Davies, C. J. Evans, P. Townsend, and P. M. Woodison, Proc. IEE 124, 179 (1977).

(11) K. Yoshida and H. Tagashira, J. Phys. D. 9, 485 (1976).

(12) H. R. Griem, Plasma Spectroscopy McGraw-Hill, New York (1964), Chapt. 4.

(13) H. Horhmann, Z. Physik. 97, 539 (1935).

(14) M. P. Freeman and S. Katz, J. Opt. Soc. Am. 50, 826 (1960).

(15) D. R. Pacquette and W. L. Wiese, Appl. Opt. 3, 291 (1964).

(16) R. J. Crumley, Thesis, Texas Tech University, 1979.

(17) H. Tholl, Z. Naturforshg, 22a, 1068 (1967).

(18) J. Koppitz, Z. Naturforshg 22a, 1089 (1967).

(19) R. A. Freeman and J. D. Craggs, J. Phys. D 2, 421 (1969).